

Influence of Ocean Surface Conditions on Atmospheric Vertical Thermodynamic Structure and Deep Convection

RONG FU

Jet Propulsion Laboratory, California Institute of Technology, Pasadena, California

ANTHONY D. DEL GENIO AND WILLIAM B. ROSSOW

NASA/Goddard Space Flight Center, Institute for Space Studies, New York, New York

(Manuscript received 26 April 1993, in final form 18 October 1993)

ABSTRACT

The authors analyze the influence of sea surface temperature (SST) and surface wind divergence on atmospheric thermodynamic structure and the resulting effects on the occurrence of deep convection using National Meteorological Center radiosonde data and International Satellite Cloud Climatology Program data for July 1983–July 1985. The onset of deep convection requires not only the existence of positive convective available potential energy (CAPE), but also an unstable planetary boundary layer (PBL). A stable PBL is observed to suppress deep convection even when CAPE is positive. Variations of SST have a major effect on CAPE, but surface wind divergence can also affect deep convection by changing the lapse rate in the lower troposphere and humidity in the PBL. Specifically, when $SST \geq 28^{\circ}\text{C}$, CAPE is always positive, and surface wind divergence does not qualitatively change the buoyancy profile above the PBL. Strong surface wind divergence, however, stabilizes the PBL so as to suppress the initiation of deep convection. In warm SST regions, $CAPE > 0$ regardless of assumptions about condensate loading, although the pseudoadiabatic limit is more consistent with the observed deep convection than the reversible moist-adiabatic limit under these circumstances. When $SST < 27^{\circ}\text{C}$, CAPE is usually negative and inhibits convection, but strong surface wind convergence can destabilize the inversion layer and moisten the PBL enough to make the atmosphere neutrally stable in the mean. As a result, deep convection is generally enhanced either when $SST \geq 28^{\circ}\text{C}$ in the absence of strong surface wind divergence or when strong surface wind convergence occurs even if $SST < 27^{\circ}\text{C}$. The anomalous suppression of deep convection in the warm area of the equatorial west Pacific lying between the ITCZ and SPCZ is probably caused by dryness in the PBL and an inversion in that area.

The seasonal cycles of deep convection and surface wind divergence are in phase with the maximum solar radiation and lead SST for one to three months in the central Pacific. The change of PBL relative humidity plays a critical role in the changeover to convective instability in this case. The seasonal change of deep convection and associated clouds seems not to have important effects on the seasonal change of local SST in the central Pacific.

1. Introduction

Deep convection plays a crucial role in coupling the tropical atmosphere and ocean systems: absorption of sunlight by the ocean is modulated by convective cloudiness; latent cooling of the surface appears as latent heating of the atmosphere by convective precipitation; atmospheric heating is enhanced by cloud and water vapor absorption of downwelling shortwave radiation and longwave radiation upwelling from the surface and boundary layer; and precipitation and evaporation form a net freshwater flux at the ocean surface. Although deep convection depends on the at-

mospheric vertical buoyancy profile and is parameterized as a function of the buoyancy profile in GCMs, most observational studies have concentrated on the relationships between large-scale ocean surface conditions and deep convection (Bjerknes 1969; Cornejo-Garrido and Stone 1977; Gadgil et al. 1984; Graham and Barnett 1987; Weare 1987; Gutzler and Wood 1990; Fu et al. 1990; Inoue 1990; Zhang 1993). While these studies have made an important contribution to the theoretical understanding and parameterization of deep convection, they are not sufficient, as it is not clear to what extent the vertical buoyancy profile is affected by surface conditions and how changes of vertical buoyancy profile affect deep convection. For example, from the fact that deep convection is suppressed when surface wind divergence ($\nabla \cdot \mathbf{V}_s > 0$) occurs, we cannot determine whether deep convection is suppressed by the presence of an inversion above the plan-

Corresponding author address: Dr. Rong Fu, Geophysical Fluid Dynamics Laboratory, Princeton University, Forrestal Campus, U.S. Route 1, P.O. Box 308, Princeton, NJ 08542.

etary boundary layer (PBL) or by a stable PBL. Therefore, investigations of the influence of large-scale surface conditions on the atmospheric vertical buoyancy profile and the occurrence of deep convection are necessary to explain the relationship observed in previous studies and to improve our understanding of the mechanisms that control deep convection.

Previous studies of radiosonde data imply that changes in large-scale surface conditions may have a significant influence on the atmospheric vertical thermodynamic structure and thus on deep convection. For example, Garcia et al. (1986) documented dramatic changes in vertical thermodynamic structure in the equatorial east Pacific between different phases of the El Niño–Southern Oscillation (ENSO) cycle that affect the redistribution of large-scale deep convection during El Niño. Firestone and Albrecht (1986) and Kloesel and Albrecht (1989) found that 60% of non-convective soundings are associated with the appearance of a trade cumulus inversion in the equatorial central Pacific during the First GARP Global Experiment (FGGE) period. Their analyses suggested a significant statistical linkage between deep convection and vertical thermodynamic structure in that area. Most earlier studies, however, are limited to relatively small areas and short time periods in which ocean surface conditions are more or less constant. Systematic changes of vertical thermodynamic structure with varying surface conditions and their impact on the occurrence of deep convection on a large scale have not been so thoroughly documented. There are a number of open questions: How do SST and surface wind divergence affect the vertical buoyancy profile? Specifically, do they affect conditional instability of the entire troposphere or only the lower atmosphere? Are changes of the vertical buoyancy profile caused mainly by changes of temperature lapse rate or humidity in the PBL? What roles do the bulk conditional instability of the atmosphere, the strength of inversions, and the instability of the PBL play in determining the large-scale distribution of deep convection? Are changes of humidity in the PBL or the lapse rate more important to changes of deep convection?

Changes of deep convection also alter clouds and the surface wind, which affect SST by changing surface latent and solar heat fluxes and ocean mixing and dynamics. Thus, examination of climatological averages or mean spatial relationships between deep convection and surface conditions cannot separate the influence of the surface conditions on the occurrence of deep convection from the feedbacks of deep convection on the surface conditions. Examination of the temporal evolution of deep convection and surface conditions may reveal the cause and effect relationship for deep convection variations. A convenient example is the seasonal cycle, which reveals the response of deep con-

vection to changes in the latitudinal distribution of solar irradiance.

In this paper, we examine these questions using collocated satellite and conventional observations of deep convection, vertical thermodynamic structure, and surface conditions (SST, wind, and humidity) in the tropical Pacific. The datasets and analysis methods are described in section 2. In sections 3 and 4, respectively, we present results for the mean state and seasonal variations. Discussion and conclusions are in sections 5 and 6, respectively.

2. Data and analysis methods

a. Data

The International Satellite Cloud Climatology Project (ISCCP) cloud data (Rossow and Schiffer 1991), National Meteorological Center (NMC) radiosonde data, Climate Analysis Center (CAC) SST data (Reynolds 1988), and The Florida State University (FSU) surface wind data (Goldenberg and O'Brien 1981) are used to diagnose deep convection, atmospheric vertical thermodynamic structure, SST, and surface wind divergence, respectively. ISCCP cloud (C1) data provide global distributions of the amounts and radiative properties of clouds, the atmosphere, and the surface every three hours (Rossow et al. 1991). Clouds are classified according to the cloud-top pressure (PC) and optical thickness (TAU) in the daytime or according to PC in the nighttime.

The NMC radiosonde dataset gives vertical profiles of temperature, dewpoint depression, and zonal and meridional wind at available stations one to four times per day. In our analysis, six stations (Fig. 1), that sample a variety of convective regimes in the tropical Pacific basin (25°S–25°N, 129°E–90°W) are used with data covering the period July 1983–July 1985. Koror and Majuro Islands are located in the intertropical convergence zone (ITCZ) year-round. Guam Island is in the ITCZ in northern summer and outside of the ITCZ in northern winter. Pago Pago is in the South Pacific convergence zone (SPCZ). Tarawa Island is in a warm SST, but infrequently convecting, area in the west Pacific during the two years analyzed. Socorro Island is in the warmest SST area in the eastern Pacific. The radiosonde measurements are reported for 20 mandatory levels and on some additional levels. Thus, the vertical resolution varies from sounding to sounding. In our analysis, the vertical profiles are linearly interpolated to 10-mb resolution from 1000 to 700 mb and to 50-mb resolution from 700 to 100 mb. A linear interpolation from the adjacent layers is applied if there is no measurement in that layer. Consistency tests, which exclude values beyond ± 5 standard deviations of the monthly means, are applied to all instantaneous soundings to remove unreasonable measurements.

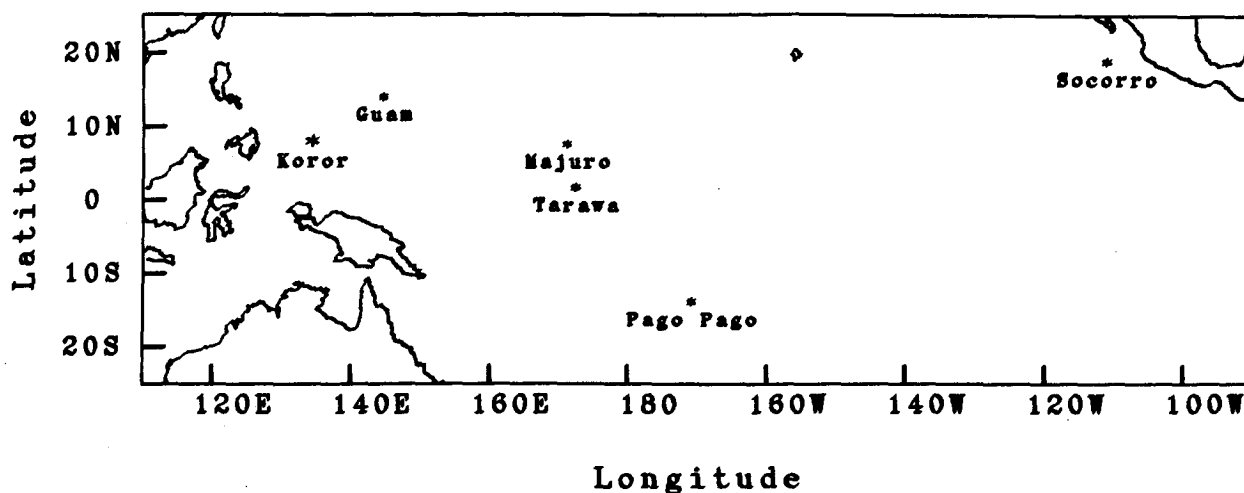


FIG. 1. The domain studied in this paper. Locations of the radiosonde stations used in the analysis are marked by *.

We use data for the period July 1983–July 1985 to study the mean deep convection, vertical buoyancy, and surface conditions and for July 1983–June 1990 for the seasonal variation analysis. The figures are monthly means of all data that pass the quality tests.

b. Analysis methods

1) IDENTIFICATION OF DEEP CONVECTION

Fu et al. (1990) applied a visible–infrared (VS–IR) threshold method to satellite radiance images (ISCCP stage B3 data) at local noon to diagnose the large-scale behavior of deep convective clouds (DCC). While this method may underestimate DCC amount by mistaking small-scale, upper-level clouds that cover only part of a satellite pixel as being lower-level and less optically thick cloud, everything selected by this method is likely to be DCC. In this paper, we generally use ISCCP C1 daytime data in which cloudy pixels with $\text{TAU} \geq 22.6$ and $\text{PC} \leq 440$ mb are identified as DCC. The DCC amount is defined as the number of DCC pixels divided by the total number of pixels within each map grid cell. The index so defined isolates DCC from other high-level clouds and presumably is a better proxy for the location of convective precipitation and latent heat release than the more widely used outgoing longwave radiation (OLR) indices (Fu et al. 1990; cf. Waliser et al. 1993).

The ISCCP C1 DCC statistics are based on coarser TAU–PC resolution and are reported at coarser spatial resolution than was used for the original study. We compared the daily variation of DCC amounts in individual map grid cells obtained from ISCCP C1 data to that obtained by the VS–IR method from ISCCP B3 data in the same ISCCP C1 map grid cell to check consistency (Fu 1991). The two methods indicate the

same spatial and temporal behavior of DCC, although the instantaneous amount of DCC is slightly different (by 10% or less). Our interest is in patterns of variation rather than absolute amounts of DCC.

At Socorro Island, where only nighttime radiosonde measurements are available (12 UTC), a PC-only threshold method is used to detect DCC: cloudy pixels with $\text{PC} \leq 310$ mb are defined as DCC. Correlations of DCC amounts determined by the TAU–PC method and the PC-only method at 0 GMT for each map grid cell in the east Pacific in February 1984 show a linear relationship with a least-square fit slope of about 1.2 (Fu 1991). This indicates that the PC-only method overestimates (by $\approx 20\%$) DCC amount relative to the TAU–PC method. Study of the diurnal cycle of DCC in the B3 data (see Fig. 8 in Fu et al. 1990) indicates that the diurnal variation of DCC top temperature is about 2 K or less. Also, the diurnal variation of DCC amount itself is small. Thus, the diurnal variation will not affect the results obtained by a fixed PC threshold method.

2) CALCULATION OF THERMODYNAMIC QUANTITIES

Relative humidity (RH), water vapor mixing ratio (q), potential temperature (θ), equivalent potential temperature (θ_e), saturation equivalent potential temperature (θ_{es}), buoyancy (B), are calculated from pressure (p), temperature (T), and dewpoint depression ΔT_d , available in the original radiosonde data. Here, θ , θ_e , and θ_{es} are calculated by the empirical formulas given by Bolton (1980) that incorporate the temperature and humidity dependence of latent heat. Term B is defined as the virtual temperature difference between an air parcel (T_{vp}) and the environment (T_{va}) following Xu and Emanuel (1989). The value of T_{vp}

depends on whether condensate loading is included and on the choice of the level from which the air parcel is lifted (which controls the initial virtual temperature). In a pseudoadiabatic process, all condensed water falls out of the air parcel immediately and does not affect the buoyancy of the parcel. In a moist-adiabatic process, all condensed water is retained in the parcel, which reduces the parcel buoyancy. How much condensed water actually falls out as rain is not easily predicted because of the lack of data on the vertical distribution of precipitation. To assess the sensitivity of our results to condensate loading, the buoyancy is estimated by both extreme assumptions. The vertical profiles of B and convective available potential energy (CAPE) are given by

$$(B_k)_i = (T_{vpk} - T_{va})_i$$

$$\text{CAPE}_k = \sum [(B_k)_i \Delta(\ln P)_i],$$

where i represents the i th pressure level, and $k = 1, 2$ represents the pseudoadiabatic process and moist-adiabatic process, respectively. The vertical integration of CAPE is from 1000 mb to 150 mb in this paper. It represents the net potential energy of atmosphere column as a result of potential energy available to convection, minus that needed to initiate convection.

The instantaneous soundings at 0 GMT are combined with instantaneous cloud observations at the same time in $2.5^\circ \times 2.5^\circ$ map grid cells containing the radiosonde stations and sorted according to the DCC frequency (cf. Tollerud and Esbensen 1985). A deep convective sounding is identified by a fractional DCC amount $\geq 10\%$,¹ representing a covered area of at least $(90 \text{ km})^2$, which is comparable to or smaller than the typical size of the active region of a convective complex (Houze 1982). Otherwise, the sounding is labeled as non-deep convective. Deep convective soundings, non-deep convective soundings, and all soundings are averaged to get monthly mean profiles for deep convectively disturbed, undisturbed, and overall conditions, respectively.

3. Influence of surface conditions on occurrence of deep convection

We examine the relationship of SST and surface wind divergence variations on tropospheric conditional instability, a necessary condition for deep convection, and instability of the PBL, which determines whether an air parcel can rise to the level of free convection (LFC), the sufficient condition for occurrence of deep convection. Following the work of Gadgil et al. (1984) and Graham and Barnett (1987), Fu et al. (1990) clas-

sified the tropical Pacific into nine SST-surface wind divergence ($\nabla \cdot \mathbf{V}_s$) regimes (see Fig. 3a for the definition of these regimes) and found systematic variations of deep convective frequency among them. To explain Fu et al.'s finding, we consider three different views of the same problem. In section 3a, we study the geographic distribution of DCC, SST, and surface wind divergence and their relationship to CAPE. The influence of variations of SST and surface wind divergence on the vertical buoyancy profiles is examined in section 3b. In section 3c, we discuss the causes of anomalous suppression of deep convection in some parts of the equatorial west Pacific warm pool from a case study.

a. Mean deep convection, surface conditions, and CAPE

Figure 2 presents maps of the DCC amount, SST, and surface wind divergence distributions for the canonical months of the four seasons in the tropical Pacific during the period October 1984–July 1985. In October 1984 (Figs. 2a and 2b), an intensive DCC zone from 5°N to 15°N extended across the whole Pacific basin, coincident with warm SSTs ($\geq 28^\circ\text{C}$). West of 170°E the intensive convection area extended poleward to 20°N . Near the equator within the warm pool, there were few DCC between the northern and southern branches of intensive convection. The south branch of intensive DCC was weaker than the northern branch but covered a broader area (5°S – 25°S , 150°E – 140°W) than the area covered by warm SST ($\geq 28^\circ\text{C}$). The southern branch of intensive DCC was collocated with an area of strong convergence, both of which were located south of the warm pool area (SST $\geq 28^\circ\text{C}$) at latitudes where the meridional gradient of SST was very large.

In January 1985 (Figs. 2c,d), the northern branch of intensive DCC had shifted equatorward to 5°N – 10°N and become narrower and weaker. It disappeared entirely in the central Pacific. The southern branch had become stronger and expanded eastward to 130°W . Southern Hemisphere SSTs had increased so that warm SSTs, strong surface wind convergence, and intensive DCC overlapped. Note that the DCC and surface wind convergence patterns formed in the south before SSTs warmed.

By April 1985 (Figs. 2e,f), the southern branch of intensive DCC had decayed, and the northern branch was reestablished. In the eastern Pacific and south of the equator, the cold SST tongue withdrew to southeast of 110°W and 10°S , and the intensive DCC area expanded to 110°W . While the warm SST pool remained in the Southern Hemisphere, the northern branch of convection became more intensive (greater DCC amount) than the southern branch and expanded poleward into cooler regions with larger SST gradients. Unlike the SPCZ in October 1984, however, the north-

¹ Varying the criterion from 10% to 30% does not change our results qualitatively.

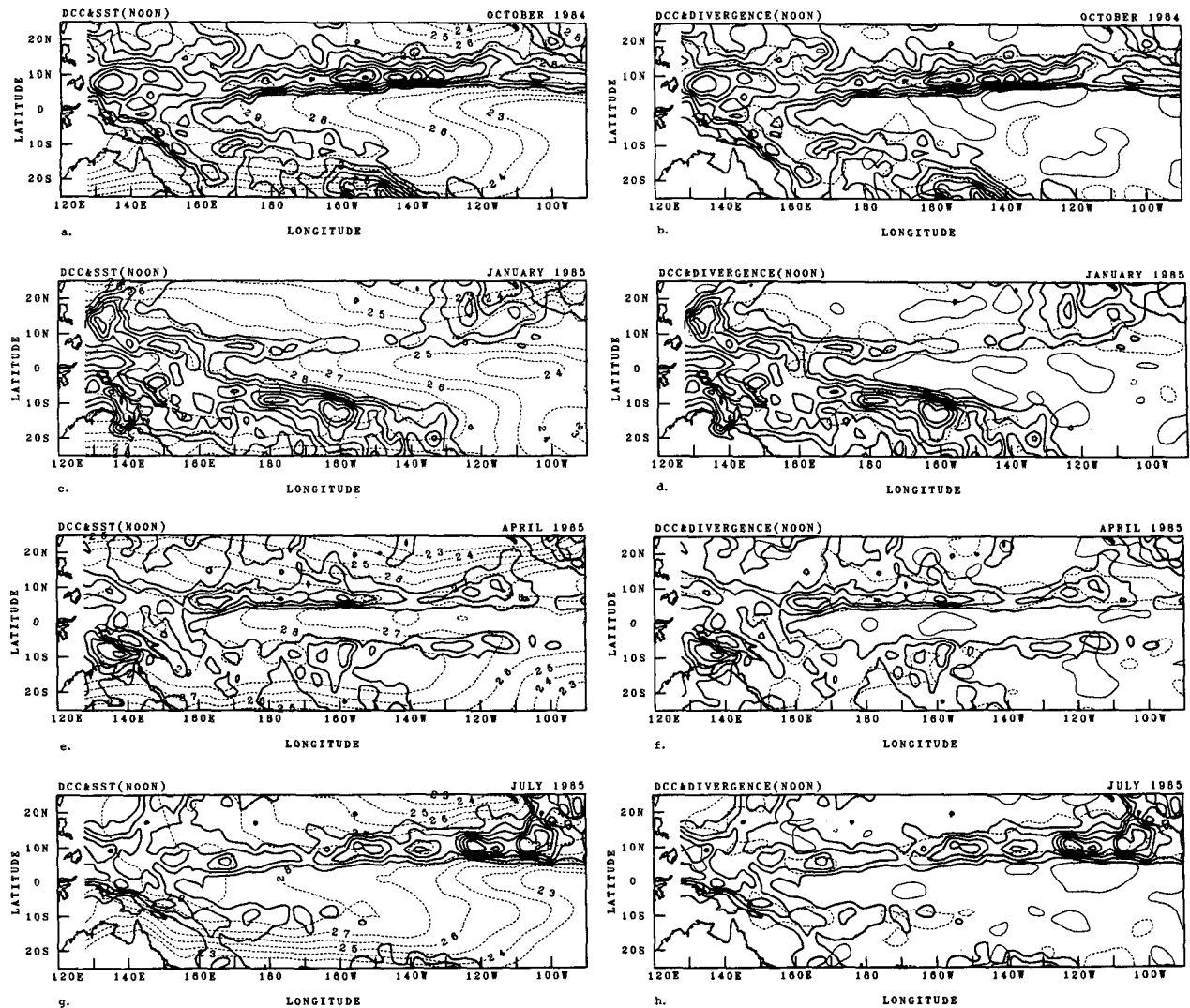


FIG. 2. (a) Distribution of DCC obtained from the TAU-PC method in October 1984. The solid contours (interval 4%) represent the monthly DCC amount averaged over a $2.5^\circ \times 2.5^\circ$ grid box. The dashed contours represent monthly mean SST ($^\circ\text{C}$). (b) Surface wind convergence and DCC amount as in (a). The areas surrounded by thin solid contours are strong divergence areas; the areas surrounded by dashed contours are strong convergence areas. (c) As in (a) but for January 1985. (d) As in (b) but for January 1985. (e) As in (a) but for April 1985. (f) As in (b) but for April 1985. (g) As in (a) but for July 1985. (h) As in (b) but for July 1985.

ern ITCZ was at least partly collocated with the warmer SSTs. In July 1985 (Figs. 2g,h), the southern branch of intensive DCC was greatly diminished and SST decreased. The northern branch was well established and collocated with the local SST maximum. Again, strong surface wind convergence and intensive convection appeared in the Northern Hemisphere *before* the warmer SSTs.

Figure 2 suggests that the relationship of convection to SST and surface wind divergence is complex. To quantify it, we plot a measure of convection enhancement versus SST-divergence regime in Fig. 3b. The regimes shown in Fig. 3a are defined according to extreme values (warm/cool, convergent/divergent) of the

parameters, separated by transition regimes with widths based on estimates of the accuracy of the data ($\pm 0.5^\circ\text{C}$ for SST, $\pm 5 \times 10^{-6} \text{ s}^{-1}$ for surface divergence). The DCC index in Fig. 3b is defined as the fractional DCC frequency (DCC pixels in each regime divided by total number of DCC pixels) normalized by the fraction of the total number of image pixels in that regime (Fu et al. 1990). Thus, in a given regime, when deep convection is enhanced (the frequency of DCC is higher than that of a random distribution), the DCC index is greater than 1. When deep convection is suppressed, the DCC index is less than 1. Figure 3b shows that deep convection is enhanced where SST is warmer than 28°C but without strong surface wind divergence (re-

gimes 7 and 8) or where strong surface wind convergence occurs even though $SST < 28^{\circ}\text{C}$ (regimes 1 and 4). The behavior in the warm SST regimes was previously inferred from OLR data by Graham and Barnett (1987). The enhancement of convection at cool SSTs has not heretofore been documented and suggests that temperature is not strictly a necessary condition for deep convection to occur.

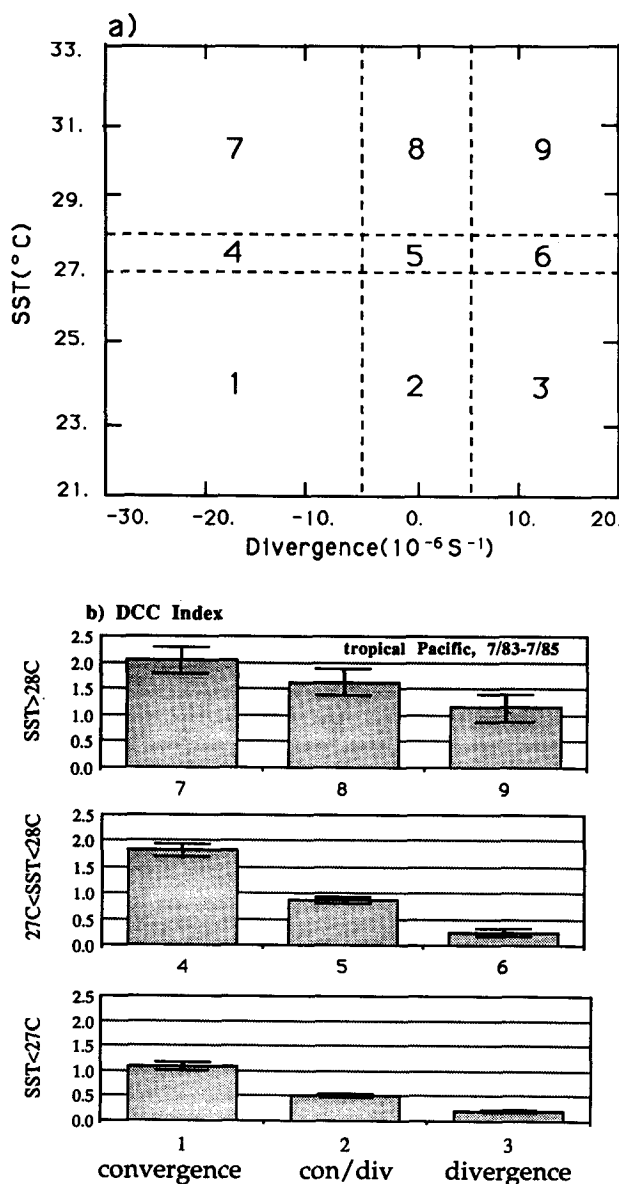


FIG. 3. (a) Definition of SST-divergence regimes. The numbers in the boxes are those indicated along the abscissas in (b). (b) The DCC index defined in Fu et al. (1990) as a function of regime for the tropical Pacific for July 1983–July 1985 obtained by the TAU-PC method. Error bars are 95% confidence intervals estimated by assuming a binomial distribution of extensive DCC pixels for the nine regimes.

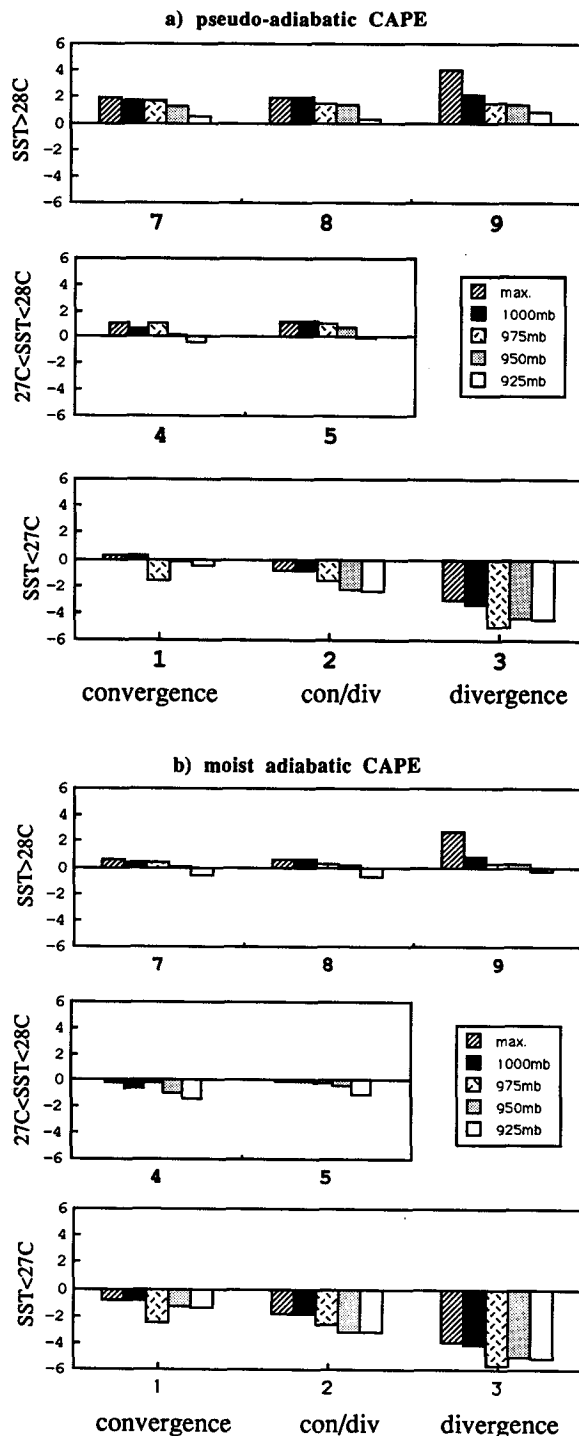


FIG. 4. (a) CAPE (kJ kg^{-1}) as a function of the SST-surface wind divergence regimes (Fig. 3a). CAPE is estimated from the mean vertical profiles of buoyancy without condensate loading for each regime in the tropical Pacific for July 1983–July 1985. The five different bars represent the maximum CAPE (see text for explanation), and the CAPE is obtained by assuming the air parcel is lifted from 1000, 975, 950, and 925 mb, respectively, as indicated in the figure. No data are available for regime 6. (b) As in (a) but for the CAPE with condensate loading.

In Fig. 4, we show the variation of monthly mean CAPE without (Fig. 4a) and with (Fig. 4b) condensate loading in the same SST–surface wind divergence regimes. The regime is defined by the monthly SST and surface wind divergence in the grid box that contains the radiosonde station. According to Xu and Emanuel (1989), the uncertainty of individual buoyancy profiles due to instrumental errors ranges from 0.6 K at 1000 mb to 1.5 K at 300 mb. The uncertainty of instantaneous CAPE is therefore 0.5 kJ kg^{-1} . The uncertainty of mean CAPE in Fig. 4 is much smaller than this number. We considered parcels originating at 1000, 975, 950, and 925 mb but show results only for 1000 mb. Maximum CAPE is defined as that associated with a parcel originating from the level where θ_e reaches its maximum between 1000 and 800 mb, since θ_e above the 800-mb level is too low for the occurrence of DCC. CAPE generally decreases as the originating altitude of the parcel increases and as condensate loading increases. In most cases, surface air (represented by 1000 mb) is the most buoyant; in regime 9, however, the maximum CAPE is much greater than the CAPE that occurs if the parcel is lifted from the surface, implying a very stable layer just above the surface.

CAPE is positive in the warm SST regimes (regimes 7, 8, and 9), near zero where $27^\circ\text{C} \leq \text{SST} < 28^\circ\text{C}$ (regimes 4, 5, and 6), and near zero or negative when $\text{SST} < 27^\circ\text{C}$ (regimes 1, 2, and 3). Thus, deep convection is enhanced not only in most regimes with positive CAPE but also in some regimes with near-zero CAPE. In regime 9, deep convection is not significantly enhanced even though CAPE is positive. These relationships are consistent with conditional instability being a necessary but not sufficient condition for deep convection.

Since complete condensate loading produces negative CAPE in regimes 1 and 4, where convection is enhanced, the loading cannot be complete (Betts 1986; Xu and Emanuel 1989). We estimate a lower limit to the precipitation efficiency by assuming that the mean deep convective sounding for regime 1 is convectively neutrally stable (CAPE = 0): precipitation efficiency in regime 1 for July 1983–July 1985 is 0.70. This means that at least 70% of the condensed water has to fall out of the parcel in order to get CAPE = 0. Of course, the precipitation efficiency may vary vertically (Betts 1986). Thus, for a more precise estimate, careful measurements of cumulus mass flux and precipitation vertical profiles are required. It is worth noting, however, that CAPE > 0 for parcels lifted from 1000 mb in regimes 7, 8, and 9, even in the limit of reversible moist-adiabatic ascent.

b. Impact of surface conditions on the vertical buoyancy structure

To see why regime 9 is different from other regimes with CAPE > 0, we examine the vertical thermody-

namic structure. Vertical profiles of buoyancy (B) estimated from the pseudoadiabatic process, assuming for illustration that the air parcel is lifted from 1000 mb, are presented in Fig. 5 for six of the SST–surface wind divergence regimes. In regimes 7 and 8, the atmosphere is conditionally unstable above 950 mb and nearly neutral below 950 mb. The LFC is at 950 mb, the average location of the PBL top in the Tropics. These conditions are consistent with the observed enhancement of deep convection. The parcel loses buoyancy at about 250 mb, consistent with the mean altitude of DCC tops estimated from ISCCP C1 data for both warm SST and cool SST areas (not shown). In regime 9 (which occurs only at Koror in the equatorial west Pacific, 7°N , 134.5°E in this analysis), there is a strong stable layer below 960 mb. This stable layer, caused by an increase of temperature upward, suppresses deep convection in regime 9, despite positive CAPE. Where $\text{SST} < 27^\circ\text{C}$, strong surface wind convergence is sufficient to destabilize the mean state of the lower atmosphere and lift parcels past the stable layer below 970 mb to the LFC at 800 mb (Fig. 5d).

Figures 6a and 6b present differences in pseudoadiabatic buoyancy profiles associated with changing SST for the same surface wind divergence conditions. The solid curve in Fig. 6a represents the buoyancy difference, $B_7 - B_1$ (B for regime 7 minus B for regime 1), and the dashed curve represents the contribution to $B_7 - B_1$ from the difference of temperature lapse rate between regimes 7 and 1. The difference between the solid and dashed curves is mainly contributed by the PBL relative humidity changes between regimes. Figure 6a shows that as SST increases the atmosphere is slightly more stable below 960 mb but more unstable above this level. This occurs because the mixed layer is actually more nearly well mixed in warm SST areas (see Fig. 5). The surface wind convergence is sufficient in all cases to raise parcels above 960 mb, producing enhanced convection in all SST regimes. The fact that the dashed curve is almost identical to the solid curve implies that these differences in buoyancy with increasing SST are due almost entirely to lapse rate differences. In the strong divergence regimes ($B_9 - B_3$, Fig. 6b), increasing SST has qualitatively similar effects on total buoyancy, but both the increase in stability within the PBL and the increase in buoyancy above are more dramatic. Unlike $B_7 - B_1$, the PBL relative humidity difference, which affects the virtual temperature of convecting parcels, is important to $B_9 - B_3$.

The effect of surface wind divergence on convective instability for similar SSTs is illustrated in Figs. 6c and 6d. For warm SST ($B_7 - B_9$, Fig. 6c) the atmosphere is more unstable in the absence of strong divergence in the 940–980-mb layer, a critical layer for the initiation of deep convection. The difference at these levels is totally due to temperature lapse rate differences. Above 940 mb, on the other hand, the atmosphere is

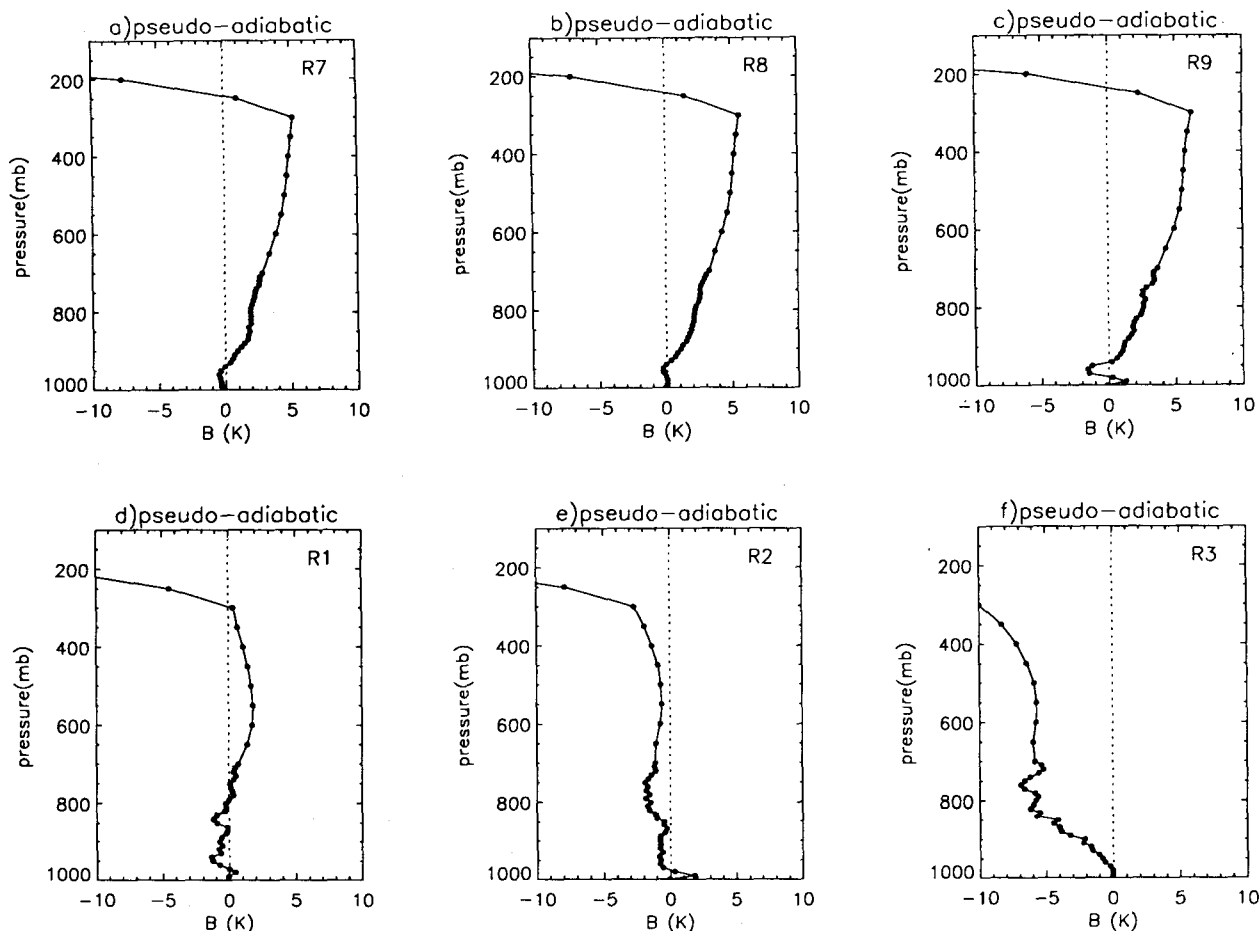


FIG. 5. The mean vertical profiles of buoyancy estimated by assuming a pseudoadiabatic process and 1000 mb as the origin level of the air parcel as a function of the SST–surface wind divergence regimes in the tropical Pacific for July 1983–July 1985. The buoyancy is defined as $T_{vp} - T_{va}$ at each pressure level, where T_{vp} and T_{va} denote the virtual temperatures of cloud parcel and atmosphere, respectively. The upper panels are for warm SST regimes ($SST \geq 28^\circ\text{C}$), and the lower panels are for cold SST regimes ($SST < 27^\circ\text{C}$). The left, middle, and right panels are for strong surface wind convergence, near-zero convergence/divergence, and strong surface wind divergence, respectively. Unit of buoyancy index: kelvin. The regime number (defined in Fig. 2a) is indicated in the upper-right corner; for example, R7 denotes regime 7. The dotted line indicates zero buoyancy.

slightly more stable in convergent areas than in divergent areas, mostly as a result of PBL relative humidity differences. In the areas of cool SST ($B1 - B3$, Fig. 6d), B increases greatly from the strong surface wind divergence case to the strong convergence case. These increases are due to both lapse rate and PBL relative humidity differences above 950 mb. Below 950 mb, the lapse rate difference is dominant.

c. DCC suppression by PBL conditions over the west Pacific

In section 3b, we have shown a statistical relationship between deep convection, vertical thermodynamic structure, and local surface conditions. Exceptions to this relationship also exist. For example, in the western Pacific warm pool ($SST \geq 28^\circ\text{C}$) in January 1994 there

was relatively little deep convection at $5^\circ\text{S} - 5^\circ\text{N}$ between the northern and southern branches of the intensive DCC zones (Figs. 7a and 7b). Figures 2c and 2d show that this situation is not unusual. The typical surface condition in that area is $SST \geq 28^\circ\text{C}$ and near-zero surface wind divergence (regime 8). Regime 8 normally has enhanced deep convection (Fig. 3b), so the normal regime 8 surface conditions alone cannot explain the absence of deep convection.

The distributions of DCC frequency and water vapor in the 1000–800-mb layer from the ISCCP C1 version of the TOVS (TIROS Operational Vertical Sounder) data in January 1984 show a pattern of low-level precipitable water that generally followed the SST except in the western Pacific warm pool near the equator, where a dry tongue extended from the eastern Pacific cold SST area (Fig. 7b). This dry tongue was collocated

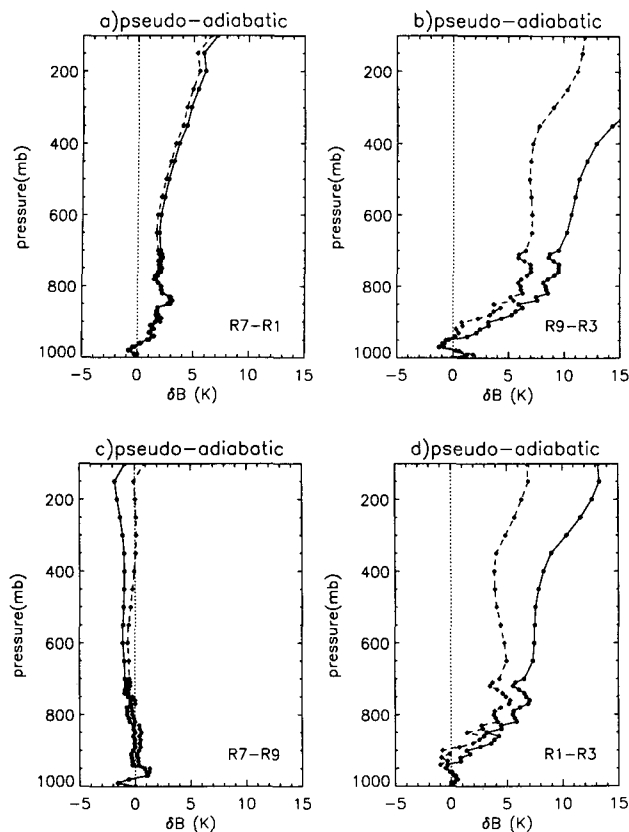


FIG. 6. Vertical profiles of total buoyancy difference (solid curve, unit: kelvin) and the buoyancy difference due to lapse rate change alone (dashed curve) between pairs of SST-surface wind divergence regimes in the tropical Pacific for July 1983–July 1985. The top panels (a, b) show differences between warm SST ($\geq 28^\circ\text{C}$) and cool SST ($< 27^\circ\text{C}$) regimes for strong convergence and divergence, respectively. The lower panels (c, d) show the difference between strong surface convergence and divergence regimes for warm SST and cool SST, respectively. The results are for pseudoadiabatic ascent from 1000 mb but are insensitive to condensate loading and parcel origin assumption.

with the near-equatorial nonconvective area. To see whether this anomalous drying might explain the suppression of convection, we compare radiosonde data from Majuro Island, which was inside an intensive DCC zone (regime 7) and Tarawa Island, which was in regime 8 but with little deep convection in this month.

Figure 8 shows the monthly mean vertical profiles of θ_e and θ_{es} for Majuro and Tarawa. The θ_{es} profile of Majuro (Fig. 8a) indicates that the atmosphere was conditionally unstable up to 300 mb, although it was locally stable ($d\theta_{es}/dz > 0$) between 800 and 700 mb. Value θ_e below the 950-mb level was high enough for air in the PBL to be unstable to deep convection compared to the θ_{es} above the PBL. This is consistent with frequent convection at Majuro. At Tarawa, however (Fig. 8b), the atmosphere was conditionally stable for

parcels lifted from any level above the surface. Value θ_e from 990 to 950 mb was about 10–15 K lower than that at Majuro (Fig. 8c), while θ_{es} differences in this layer were negligible. This low θ_e in the PBL apparently prevented deep convection at Tarawa. The presence of the inversion layer between the 900 and 800 mb levels, perhaps as a result of subsidence introduced by the ITCZ (Hack et al. 1989; Schubert et al. 1991), reinforced the conditional stability. At Tarawa (Fig. 9), RH was about 10%–25% less and q about 4 g kg^{-1} less than at Majuro in the whole trade cumulus layer (1000–800 mb). We have crudely estimated the evaporation from the SST and surface wind data using the standard bulk formula (Fu et al. 1990) and find that it was even higher in the dry tongue area than in the moist, strongly convecting SPCZ area. Thus, large-scale moisture transports must cause the dryness in the PBL. East of 165°E , an area of surface wind divergence (Fig. 7c) is collocated with the dry tongue, where the dryness may be caused by subsidence. West of 165°E , the dry tongue cannot be explained by subsidence because only weak surface wind convergence occurs (Fig. 7c). An alternative possibility is horizontal moisture advection: easterly winds (Fig. 7c) and the longitudinal precipitable water gradient (Fig. 7b) suggest that dry air was advected from the east. Assuming a PBL adjustment time of 1–2 days (Schubert et al. 1979), horizontal advection could have carried dry air westward an additional 10° – 15° in longitude. Combined with the results in Figs. 3 and 4, the situation in this region emphasizes the importance of nonlocal dynamical effects on the onset of deep convection.

4. Seasonal variations of DCC, SST, and surface wind divergence

The correlations shown in the previous section suggest a complex combination of thermodynamic and dynamic controls on deep convection. For more insight into the factors responsible for establishing convective regimes in the tropical Pacific, we examine the seasonal cycle of DCC, surface conditions, and associated seasonal changes in vertical structure over many years.

Figure 10 compares the seasonal variations of SST, surface wind divergence, and intensive DCC at 180° longitude for the July 1983–June 1990 period. The warm SST ($\text{SST} \geq 28^\circ\text{C}$) area reaches its southern extreme position in March and its northern extreme position in September or October (Fig. 10a), lagging the maximum solar radiation by two to three months. Seasonal variations of the surface wind convergence (Fig. 10b) and the intensive DCC (Fig. 10c) are dominated by intensification and poleward expansion of features in each hemisphere rather than cross-equatorial migration. They are almost in phase with the maximum solar radiation change. This implies that a local response to a seasonal increase of SST does not

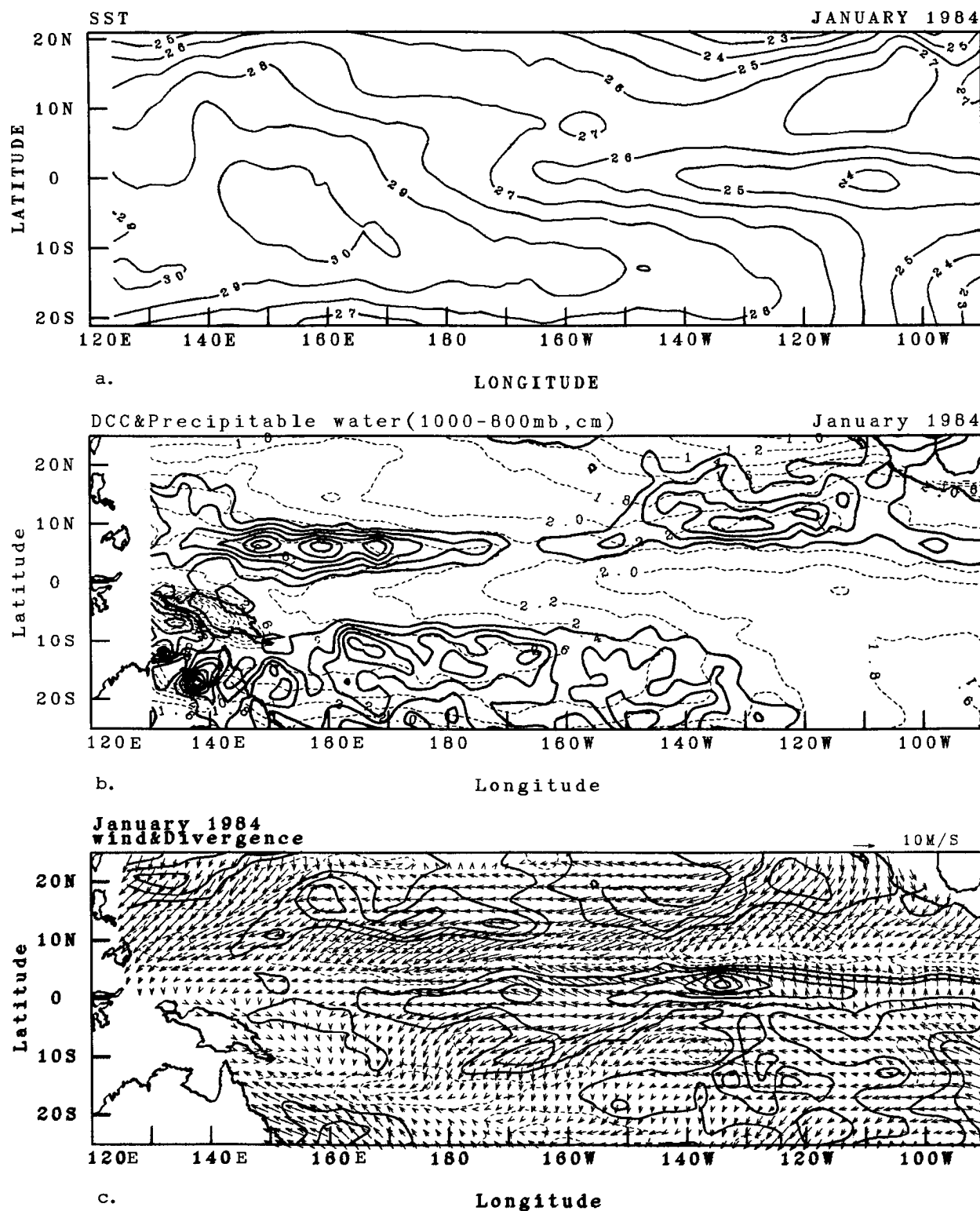


FIG. 7. (a) Distributions in the tropical Pacific for January 1984 of (a) monthly mean SST (contour interval is 1 $^{\circ}\text{C}$), (b) monthly mean DCC amount (solid contours with 4% interval), and precipitable water in the 1000–800-mb layer (dashed contours, unit: cm), (c) monthly mean surface wind velocity (arrows) and divergence (solid contours represent zero and positive divergence; dashed contours represent convergence; the contour interval is $5 \times 10^{-6} \text{ s}^{-1}$).

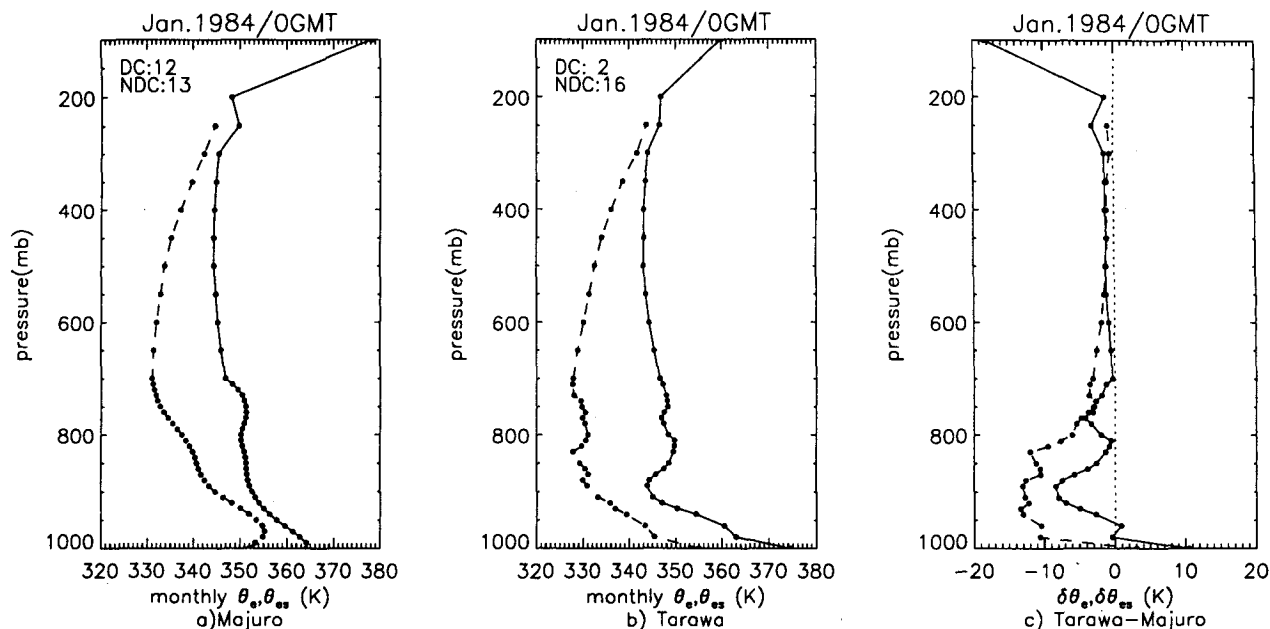


FIG. 8. (a) The monthly mean vertical profiles of θ_e (dashed curve) and θ_{es} (solid curve) at Majuro for January 1984. (b) As (a) but for Tarawa. (c) The differences of vertical profiles of θ_e and θ_{es} (Tarawa minus Majuro) for January 1984. Unit of θ_e and θ_{es} : kelvin. The numbers of deep convective and non-deep convective soundings are marked by DC and NDC in the upper-left corner of each diagram.

produce the seasonal changes in deep convection. In the Northern Hemisphere, the ITCZ and intensive DCC zone exist during most of the year. The SPCZ expands poleward to its southern extreme position in January. The southern branch of the intensive DCC appears from October to May and becomes strongest in January. From May to October, it disappears. Figure 10 confirms our impression from Fig. 2 that the seasonal variations of the surface wind convergence and the intensive DCC lead those of the warm SST by a few months in the central Pacific (180° – 140° W). Since the seasonal variations of the surface wind divergence and the intensive DCC zone are in phase with solar radiation, convection apparently responds on short timescales (<1 month) to increased solar heating and surface wind convergence.

It is of interest to see whether the seasonal convective instability change is caused primarily by temperature changes above the PBL (i.e., the large-scale environment) or by temperature and humidity changes in the PBL. Figure 11 compares the mean profiles of θ_e and θ_{es} at Pago Pago (see Fig. 1) for July 1984, October 1984, and January 1985. At Pago Pago, when the station was out of the intensive DCC zone in July 1984, the atmosphere was convectively stable for an air parcel originating anywhere above the surface (Fig. 11a). The stable condition was a result of a dry and cold PBL and a strong inversion layer from 850 to 750 mb. In October 1984, when intensive DCC appeared at the station, but before SST reached 28°C , the atmosphere

was convectively unstable (Fig. 11b) due solely to a 7-K increase of θ_e in the PBL, since θ_{es} at the surface and at the top of the inversion layer (750 mb) remained almost the same as that in July (Fig. 11d). In other words, the seasonal onset of deep convection at Pago Pago was determined solely by increasing PBL relative humidity.

By January, when SST at Pago Pago was warmer than 28°C , θ_{es} below 700 mb (Fig. 11c) had increased by more than 10 K relative to October (Fig. 11e). The increases of both θ_e and θ_{es} in the PBL created an even more convectively unstable environment, thus enhancing deep convection further (see Figs. 2a,c). From October to January, q increased by 2 g kg^{-1} in the PBL, but more than half of this was due to the SST change, according to the Clausius–Clapeyron equation (Fu 1991). We conclude that the dynamical and surface processes that regulate PBL relative humidity initiate the seasonal onset of convection, while SST effects enhance convection later in the solstice seasons.

The above behavior is a characteristic of the seasonal cycle only in the central Pacific. In the west Pacific, the seasonal variations of SST, surface wind divergence, and deep convection are mostly in phase with each other with peaks one to two months after January and July. Our results agree with the findings of Horel (1982), who observed a progressive delay of maximum SST off the equator (his Fig. 1) and a lead of surface wind convergence from west to central Pacific (his Fig. 4). Because the seasonal phase relationships of SST,

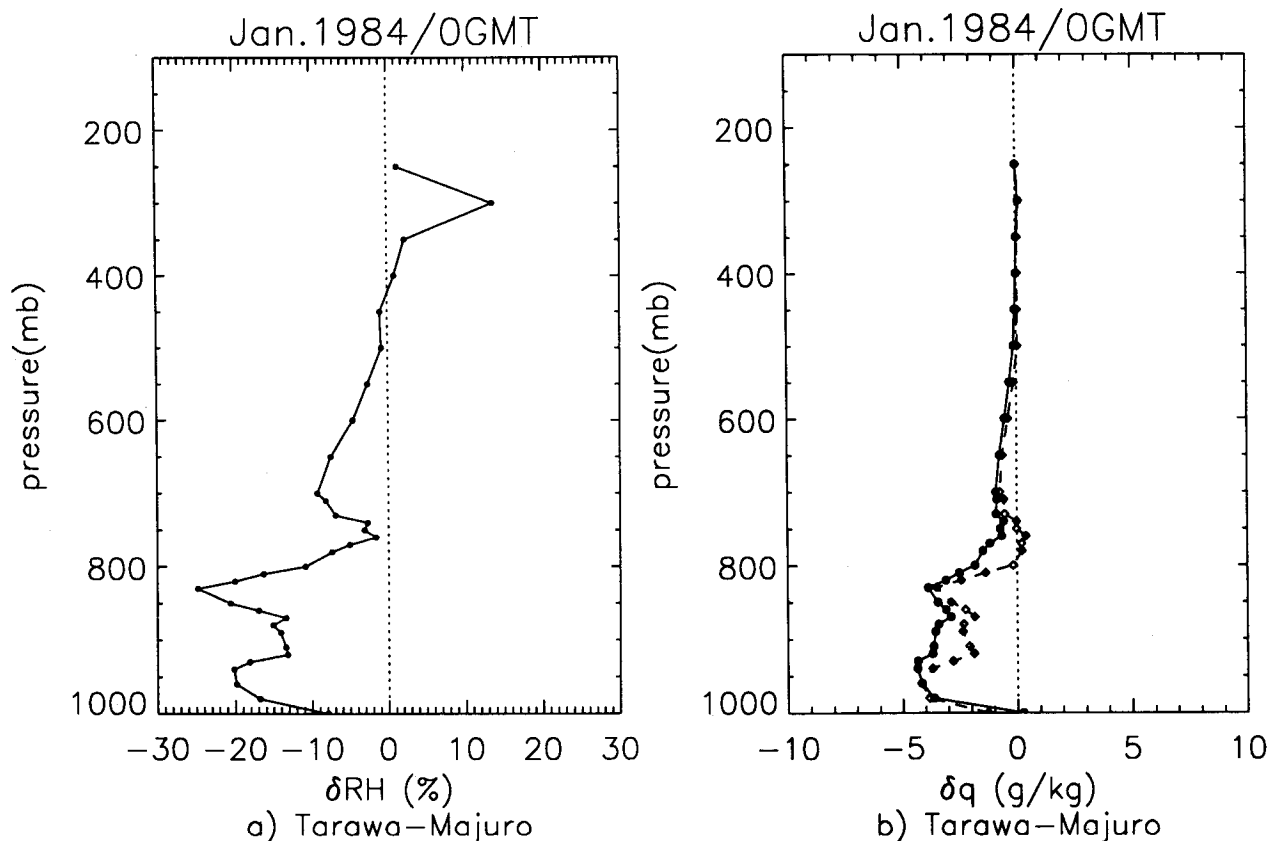


FIG. 9. (a) The difference of relative humidity profiles (Tarawa minus Majuro) for January 1984. Unit: percent. (b) The difference of q profiles between Tarawa and Majuro (solid curve) and the difference of q profiles contributed by relative humidity differences between Tarawa and Majuro (dashed curve with diamonds) for January 1984. Unit of q : gram per kilogram.

surface wind convergence, and deep convection vary longitudinally, it is not surprising that we obtain a different impression of the controlling factors than is obtained from zonal mean seasonal variations (cf. Meehl 1987). The longitudinal variation of these relationships also suggests that some other factor(s) are involved in determining the seasonal variations of DCC and SST.

5. Discussion

a. Comparison with previous studies

Our results suggest that surface wind convergence plays an important role in determining deep convection, in agreement with the results of Cornejo-Garrido and Stone (1977). We have shown that surface wind convergence promotes convection mainly through moistening and destabilizing the PBL when SST is above 28°C and through moistening and destabilizing the lower atmosphere (from surface to the inversion layer) when SST is about $25^{\circ}\text{--}27^{\circ}$. Our results agree with Gadgil et al. (1984) and Graham and Barnett (1987) that convection is enhanced in areas where SST

$\geq 28^{\circ}\text{C}$. They suggested that SST of about 28°C (T_c) is a necessary condition for deep convection onset. We found that in areas of strong surface wind divergence and $\text{SST} \geq 28^{\circ}\text{C}$, deep convection was suppressed mainly by a stable and dry PBL even though the atmosphere above the PBL was still conditionally unstable. Thus, surface wind convergence is also required for deep convection onset (Gadgil et al. 1984; Graham and Barnett 1987). Our results, however, also show that conditional instability can be achieved by strong surface wind convergence even when SSTs are relatively cool ($\sim 25^{\circ}\text{--}28^{\circ}\text{C}$). This result is different from Graham and Barnett's suggestion that "below T_c deep convection does not occur," which may be due to an underrepresentation of east Pacific cases in their analysis. For example, there are no sites east of 150°W in the tropical Pacific included in their Figs. 2, 5, and 6 and only five samples in their Fig. 4.

Neelin and Held (1987) and Lau and Shen (1988) suggested that increases of moisture in the PBL play an important role in promoting deep convection when $\text{SST} \geq 28^{\circ}\text{C}$. Our Figs. 5c, 8b, 8c, and 9 support their suggestion and also show that deep convection will be

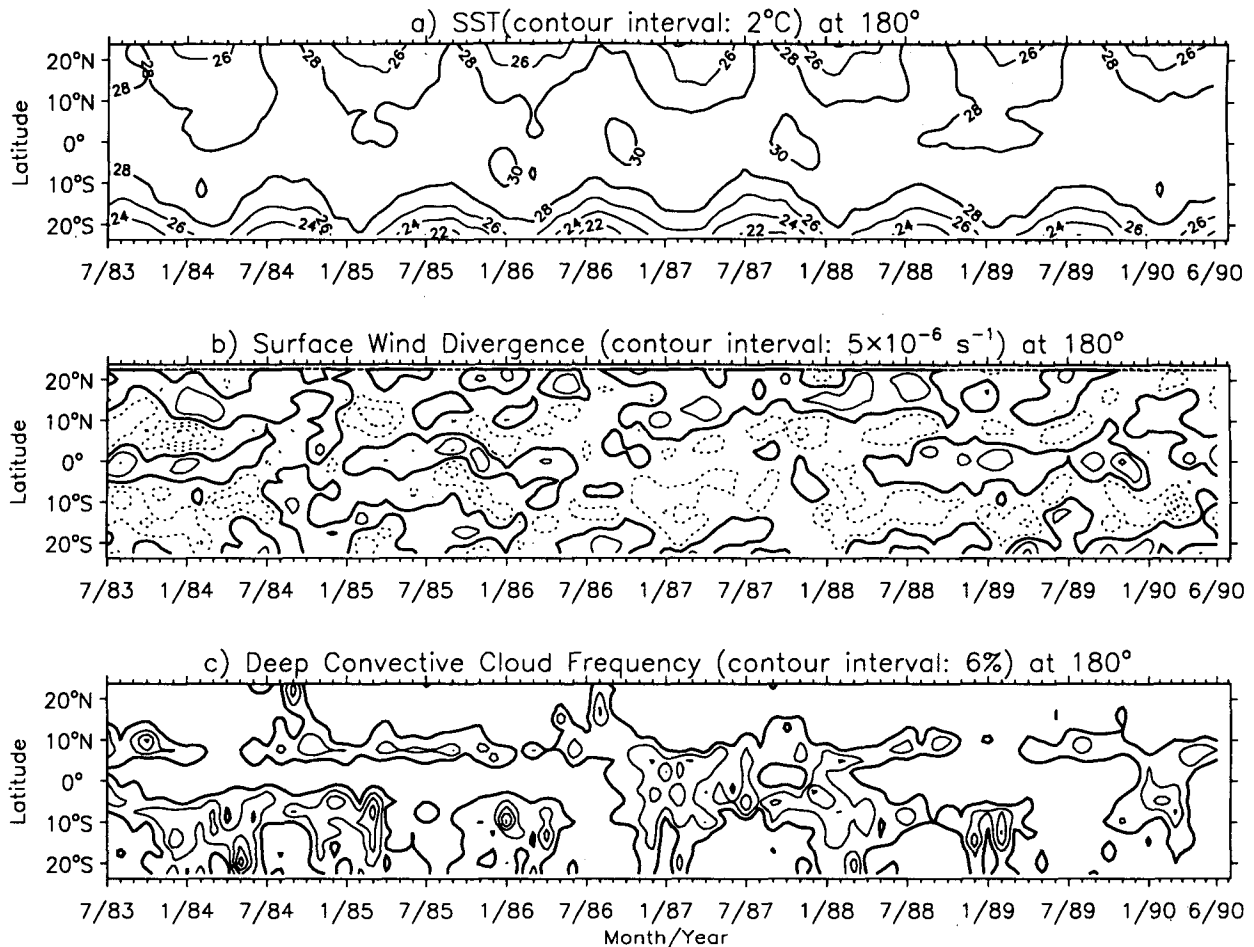


FIG. 10. Latitude–time diagrams for July 1983–July 1990 at 180°. (a) Monthly mean SST. The value of each contour is marked in °C. (b) Monthly mean surface wind divergence. The thin solid contour represents divergence and dashed contours represent convergence. Zero divergence is represented by the bold contour. The contour interval is $5 \times 10^{-6} \text{ s}^{-1}$. (c) Monthly DCC amount. The contour interval is 6% and the first contour is 6%.

suppressed if the PBL is dry enough even when $\text{SST} \geq 28^\circ\text{C}$. Our results are also consistent with Inoue's (1990) finding that deep convection is correlated with low-level moisture in the tropical west Pacific.

Compared with the central and east Pacific, the structure of the trade inversion west of the date line has not been so thoroughly documented. Based on two years of radiosonde analyses from four stations in the tropical west Pacific, our Figs. 5a and 5b indicate that the trade inversion was not visible in the mean vertical buoyancy profiles over the area of warm SST except when there was divergence.

b. Implications for cumulus and boundary-layer parameterizations

The relationship among CAPE, PBL structure, and DCC and their variations with SST–surface wind divergence regimes is illustrated in Figs. 3 to 5 and sum-

marized in Table 1. CAPE is not sufficient to predict the occurrence of deep convection because the latter depends on the details of the vertical profile of buoyancy as well. Thus, simulation of deep convection requires not only a satisfactory simulation of CAPE (large-scale circulation), but also of the vertical structures of temperature and humidity, especially in the lower troposphere and PBL. Parameterization schemes that rely solely on either CAPE or low-level wind convergence may incorrectly diagnose the presence or absence of deep convection in some situations. Figure 4 suggests that the pseudoadiabatic limit may be more reliable than the reversible moist-adiabatic limit in predicting the occurrence of deep convection in cumulus parameterizations.

Our radiosonde analysis indicates that the occurrence of deep convection is most sensitive to temperature variations in the inversion layer and PBL. It is not clear, for example, whether mixed-layer approaches

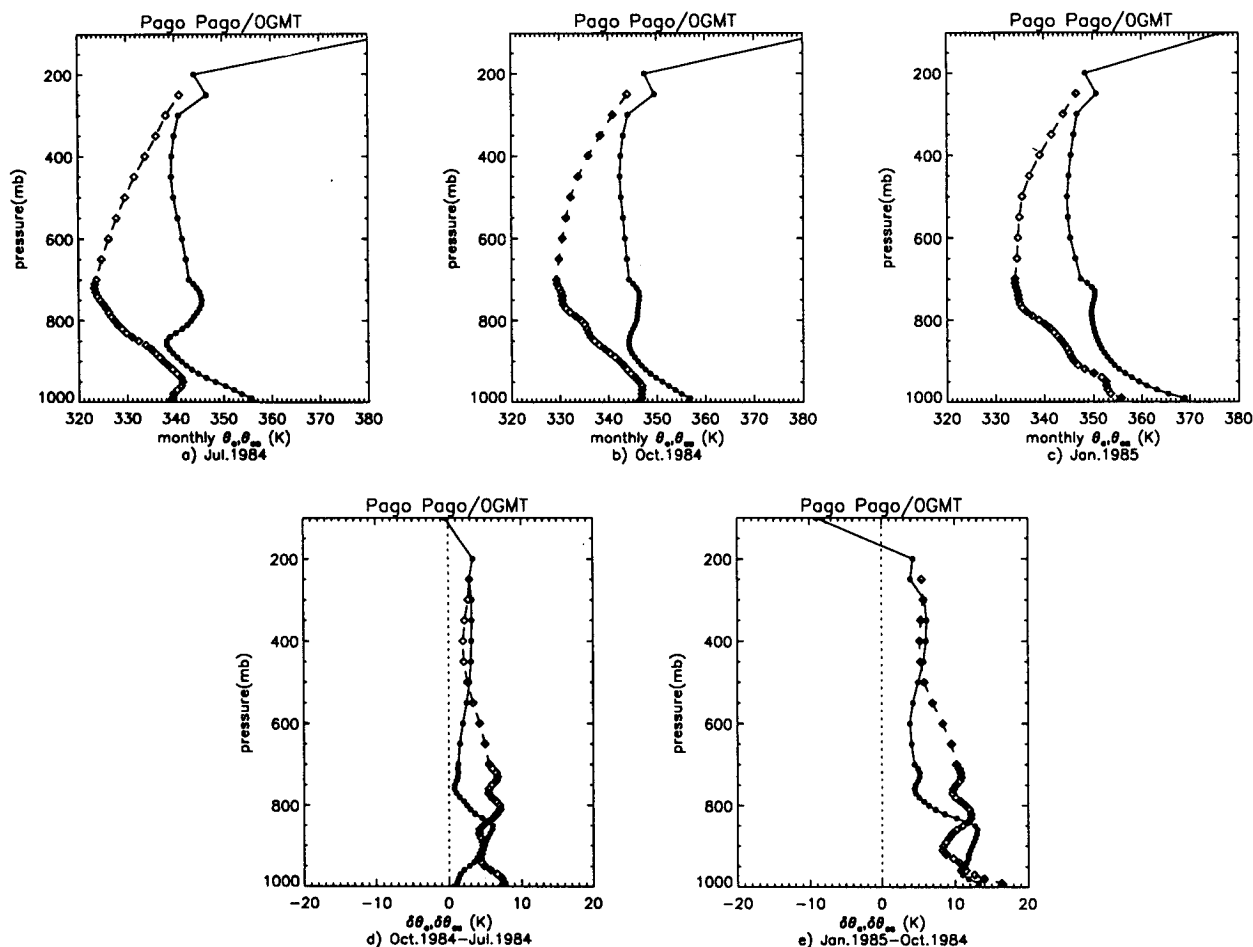


FIG. 11. The monthly mean vertical profiles of θ_e (dashed curve with diamonds) and θ_{es} (solid curve with dots) at Pago Pago for (a) July 1984, (b) October 1984, and (c) January 1985. The differences between θ_e and θ_{es} profiles of (d) October 1984 minus July 1984 and (e) January 1985 minus October 1984 at Pago Pago. Unit of θ_e and θ_{es} : kelvin.

to PBL parameterization can successfully predict the suppression of deep convection in the warm SST and divergent surface wind regime. At least two layers between the surface and 950 mb and two layers between 850 and 750 mb are needed to resolve the observed variations of PBL instability and the structure of the inversion. This suggests that the performance of current cumulus parameterizations in GCMs may be limited by their coarse vertical resolution in the trade cumulus boundary layer and PBL.

c. Implications for the SST–surface wind relationship

What controls tropical surface wind convergence? CISK theory suggests that surface wind convergence is both a cause and a result of deep convection. Thus, surface wind convergence should coincide with regions of deep convection. Neelin and Held (1987) suggest that convergence is caused by convection as a result of

increasing low-level moisture and thereby increasing instability associated with warm SST. Thus, surface wind convergence should coincide with warm SST. Lindzen and Nigam (1987) claim that convection is primarily a response to surface conditions rather than a forcing. In their view, the surface wind is mainly controlled by the SST gradient through its influence on the pressure field, so that surface wind convergence should occur in the locally warmest area where surface pressure is lowest. Wallace et al. (1989) suggest that in the SST frontal zone, cross-isobar advection tends to smooth out the pressure gradients and shift strong divergence to the downwind side of the local maximum SST area.

The seasonal variations of deep convection, SST, and surface wind divergence in the tropical Pacific (Fig. 2) show that all three parameters are collocated in the solstice seasons. In the equinox seasons, however, surface wind convergence collocates with deep convection

TABLE 1. The mean CAPE, instability of planetary boundary layer (PBL), top of the trade cumulus boundary layer (TCBL), mixed-layer depth, level of free convection (LFC), the vanishing buoyancy level (VBL), and percentage of months when DCC is enhanced (DDC index > 1) as a function of the SST–surface wind divergence regimes in the tropical Pacific.

Strong convergence	Near zero	Strong divergence
SST $\geq 28^{\circ}\text{C}$		
CAPE > 0	CAPE > 0	CAPE > 0
PBL: weak stable	neutral	strong stable
TCBP top: none	none	750 mb
mixed layer: 950 mb	950 mb	980 mb
LFC: 960 mb	960 mb	960 mb
VBL: 240 mb	240 mb	240 mb
DCC: 80% ¹ , 50% ²	90%, 55%	0%, 0%
SST $< 27^{\circ}\text{C}$		
CAPE ≈ 0	CAPE < 0	CAPE < 0
PBL: stable	stable	stable
TCBL top: 850 mb	750 mb	750 mb
mixed layer: 970 mb	970 mb	970 mb
LFC: 800 mb	none	none
VBL: 300 mb	300 mb	300 mb
DCC: 5%, 35%	0%, 0%	0%, 0%

¹ For the west Pacific.

² For the east Pacific.

but not with warm SST. The correlation between deep convection and surface wind convergence is consistent with that required by the CISK assumption but does not constitute evidence either for or against CISK-type feedbacks. The relationship between surface wind divergence and SST in the solstice seasons is consistent with that suggested by Neelin and Held and Lindzen and Nigam, and our radiosonde analysis supports the point of Neelin and Held that low-level moisture plays a key role in the change of convection and convergence. For the equinox seasons, though, convergence is not collocated with warm SST because the low-level moisture is not correlated with SST. The correlation between surface wind divergence and SST implies that the Neelin and Held and Lindzen and Nigam theories may be an appropriate description of mean or extreme conditions but do not explain the convergence pattern in equinox seasons. Figures 2 and 10 also illustrate that, while most climate analyses tend to focus on the solstice seasons, it is the equinoxes that best illustrate climate processes in action. These figures also show that zonal mean analyses oversimplify the seasonal variation (cf. Mitchell and Wallace 1992).

Figure 2 suggests that the dynamics of the SPCZ may be different from that predicted by either the Lindzen and Nigam or Wallace et al. hypotheses. Our observations are consistent with those of Kiladis et al. (1989) for Southern Hemisphere spring (October 1984) and with Storch et al. (1988) for Southern Hemisphere summer (January 1985). The former suggest that the eastern part of the SPCZ and the northwest–southeast orientation of the SPCZ are

formed by an interaction between the southern monsoon circulation, due to Australian continental heating, and the westerlies at middle latitudes. The latter found that the SPCZ during the Southern Hemisphere summer is more sensitive to underlying SST changes. The change of the behavior of the SPCZ between the Southern Hemisphere spring and summer may be caused by the southward shift of the warm SST zone, which reduces the land–sea surface temperature contrast and thus reduces the relative heating effect of the Australian continent.

d. How do deep convection and surface wind affect the seasonal variation of ocean surface heat flux?

Deep convection and surface wind affect SST primarily through their impacts on surface solar radiation, latent heat flux, and wind stress. If clouds are the primary regulator of tropical SST (cf. Ramanathan and Collins 1991), then we would expect the seasonal warming of SST to cease when deep convection and its associated highly reflective anvil clouds are established. Figure 10 shows, however, that the onset of intensive deep convection does not stop the seasonal warming of SST. This implies that the influence of clouds associated with intensive deep convection on net surface heat flux does not dominate the total seasonal change of net surface heat flux. The reason may be that the decrease of solar heating is sometimes also associated with a reduction of evaporative cooling because of weaker wind speeds in the convergence area. As an example, we compare the net heat flux difference (assumed to be solely due to changes in solar and latent heat fluxes) shown by Liu and Gautier (1990) in January 1981 and 1983 when large cloud changes occurred in the equatorial central Pacific to remove the influence of solar zenith angle on surface net heat flux. In January 1981, the combined heat flux was about 140 W m^{-2} as a net result of 250 W m^{-2} solar radiation and -100 W m^{-2} latent heat flux (their plate 1). By comparison, in January 1983, the heat flux was again about 130 W m^{-2} , but the solar flux was about 200 W m^{-2} , and the latent heat flux was about -70 W m^{-2} . This result implies that, for the same solar zenith angle, the total net surface heat flux change associated with changes in deep convection may not be sufficient to control seasonal changes of SST in that area. Since the net heat flux change depends on mean and transient states of the dynamical and radiative fields in very complicated ways, the above example may not represent a general tendency for the solar and latent heat changes over all parts of the tropical Pacific.

6. Summary and conclusions

We have examined the dependence of tropical Pacific deep convection and convective instability on

large-scale surface conditions. A TAU-PC threshold method to distinguish deep convective clouds from cirrus/anvil clouds in ISCCP C1 data is used. In lieu of more direct satellite estimates of convective precipitation, our deep convection index provides a more reliable proxy for large-scale variations in convection than conventional indices based on outgoing longwave radiation.

SST variation has a major effect on both CAPE and the vertical buoyancy profile. When $SST \geq 28^{\circ}\text{C}$, CAPE is always positive and the LFC is usually at about 960 mb. Surface wind divergence does not qualitatively change the buoyancy profile above the PBL. Very strong surface divergence, however, can stabilize and dry the PBL enough to suppress the initiation of deep convection. When $SST < 27^{\circ}\text{C}$, the atmosphere is usually convectively stable unless strong enough surface wind convergence destabilizes the inversion layer and moistens the PBL enough so that the atmosphere becomes weakly conditionally unstable or nearly neutrally stable in the mean. Thus, the necessary conditions for deep convection can be achieved either by warm SST ($SST \geq 28^{\circ}\text{C}$) or by surface wind convergence.

Because the onset of deep convection depends not only on the existence of positive CAPE, but also on the vertical profile of air parcel buoyancy, especially in the PBL, high vertical resolution in a model PBL is needed to resolve such changes of PBL instability. The absence of deep convection in the equatorial west Pacific is caused by dryness in the PBL that is probably a result of subsidence associated with surface wind divergence and easterly advection of drier air. The foregoing results indicate that dynamic conditions are also important in determining the conditions for the occurrence of deep convection. The relation between deep convection and SST is strongly influenced by variations in the large-scale circulation.

The seasonal cycles of deep convection, SST, and surface wind divergence in the central Pacific show that the latitudinal shifts of the deep convective area and the surface wind convergence area are in phase with that of the maximum solar radiation, while the warm SST ($\geq 28^{\circ}\text{C}$) area lags the seasonal cycle of the maximum solar radiation by one to two months. The seasonal variation of the occurrence of deep convection is consistent with observed changes of convective instability initiated by an increase of PBL relative humidity before SST rises to 28°C , but later enhanced by temperature increases in the PBL. Thus, the onset of deep convection responds immediately to the surface solar radiation increase and surface wind convergence instead of waiting for the rise of SST, although it is not clear whether surface wind convergence is the cause or result of the seasonal variation of deep convection. Changes in surface radiation associated with the appearance of extensive cirrus/anvil clouds do not have a dominant impact on the seasonal variation of SST.

In fact, the SST continues to rise in some areas after the onset of deep convection.

Acknowledgments. The authors are grateful to Mark Cane and Stephen Zebiak for constructive discussions and valuable suggestions that initiated the radiosonde data analysis in this paper. We thank Inez Fung, Timothy Liu, David Rind, Duane Waliser, and Kuanman Xu for helpful comments on the manuscript. We also thank Kevin Trenberth for sharing helpful information about radiosonde data and Ken Bell and Alison Walker for their help in decoding the radiosonde data. This work was supported by the NASA Tropical Rainfall Measuring Mission, the International Satellite Cloud Climatology Project, and the NASA Earth Observing System Interdisciplinary Sciences Programs at GISS and JPL.

REFERENCES

- Betts, A. K., 1986: A new convective adjustment scheme. Part I: Observational and theoretical basis. *Quart. J. Roy. Meteor. Soc.*, **112**, 677–691.
- Bjerknes, J., 1969: Atmospheric teleconnections from the equatorial Pacific. *Mon. Wea. Rev.*, **97**, 163–172.
- Bolton, D., 1980: The computation of equivalent potential temperature. *Mon. Wea. Rev.*, **108**, 1046–1053.
- Cornejo-Garrido, A. G., and P. H. Stone, 1977: On the heat balance of the Walker circulation. *J. Atmos. Sci.*, **34**, 1155–1162.
- Firestone, J. K., and B. A. Albrecht, 1986: The structure of the atmosphere boundary layer in the central equatorial Pacific during January and February of FGGE. *Mon. Wea. Rev.*, **114**, 2219–2231.
- Fu, R., 1991: Deep convection and its relationship to the large-scale circulation over the tropical Pacific. Ph.D. dissertation, 171 pp.
- , A. D. Del Genio, and W. B. Rossow, 1990: Behavior of deep convective clouds in the tropical Pacific deduced from ISCCP radiances. *J. Climate*, **3**, 1129–1152.
- Gadgil, S. P., P. V. Joseph, and N. V. Joshi, 1984: Ocean–atmosphere coupling over monsoon regions. *Nature*, **312**, 141–143.
- Garcia, O., S. J. S. Khalsa, and E. J. Steiner, 1986: Atmospheric characteristics of the equatorial Pacific during the 1982–1983 El Niño, deduced from satellite and aircraft observations. *J. Geophys. Res.*, **91**, 13 271–13 231.
- Goldenberg, S. B., and J. J. O'Brien, 1981: Time and space variability of tropical Pacific wind stress. *Mon. Wea. Rev.*, **109**, 1190–1206.
- Graham, N. E., and T. P. Barnett, 1987: Observations of sea surface temperature and convection over tropical oceans. *Science*, **238**, 657–659.
- Gutzler, D. S., and T. M. Wood, 1990: Structure of large-scale convective anomalies over tropical oceans. *J. Climate*, **3**, 483–496.
- Hack, J. J., W. H. Schubert, D. E. Stevens, and H. C. Kuo, 1989: Response of the Hadley circulation to convective forcing in the ITCZ. *J. Atmos. Sci.*, **46**, 2957–2973.
- Horel, J. D., 1982: On the annual cycle of the tropical Pacific atmosphere and ocean. *Mon. Wea. Rev.*, **110**, 1863–1878.
- Houze, R. A., Jr., 1982: Cloud clusters and large-scale vertical motions in the tropics. *J. Meteor. Soc. Japan*, **60**, 396–409.
- Inoue, T., 1990: The relationship of sea surface temperature and water vapor amount to convection over the western tropical Pacific revealed from split window measurements. *J. Meteor. Soc. Japan*, **68**, 589–606.
- Kiladis, G. N., H. V. Storch, and H. Van Loon, 1989: Origin of the South Pacific Convergence Zone. *J. Climate*, **2**, 1185–1195.
- Kloesel, K. A., and B. A. Albrecht, 1989: Low-level inversions over the tropical Pacific—Thermodynamic structure of the boundary

- layer and the above-inversion moisture structure. *Mon. Wea. Rev.*, **117**, 87–101.
- Lau, K. M., and S. Shen, 1988: On the dynamics of intraseasonal oscillation and ENSO. *J. Atmos. Sci.*, **45**, 1781–1797.
- Lindzen, R. S., and S. Nigam, 1987: On the role of sea surface temperature gradients in forcing low-level winds and convergence in the tropics. *J. Atmos. Sci.*, **44**, 2418–2436.
- Liu, T. W., and C. Gautier, 1990: Thermal forcing on the tropical Pacific from satellite data. *J. Geophys. Res.*, **95**, 13 209–13 217.
- Meehl, G. A., 1987: The annual cycle and interannual variability in the tropical Pacific and Indian Ocean regions. *Mon. Wea. Rev.*, **115**, 27–50.
- Mitchell, T. P., and J. M. Wallace, 1992: The annual cycle in equatorial convection and sea surface temperature. *J. Climate*, **5**, 1140–1156.
- Neelin, J. D., and I. M. Held, 1987: Modeling tropical convergence based on the moist static energy budget. *Mon. Wea. Rev.*, **115**, 3–12.
- Ramanathan, V., and W. Collins, 1991: Thermodynamic regulation of ocean warming by cirrus clouds deduced from observations of the 1987 El Niño. *Nature*, **351**, 27–32.
- Reynolds, R. W., 1988: A real-time global sea surface temperature analysis. *J. Climate*, **1**, 75–86.
- Rossow, W. B., and R. A. Schiffer, 1991: ISCCP cloud data products. *Bull. Amer. Meteor. Soc.*, **72**, 1–20.
- , L. C. Garder, P. J. Lu, and A. Walker, 1991: International Satellite Cloud Climatology Project (ISCCP) documentation of cloud data. WMO/TD No. 266, World Climate Research Program (ICSU/WMO), 75 pp. (plus three appendices).
- Schubert, W. H., J. S. Wakefield, E. J. Steiner, and S. K. Cox, 1979: Marine stratocumulus convection. Part I: Governing equations and horizontally homogeneous solutions. *J. Atmos. Sci.*, **36**, 1286–1307.
- , P. E. Ciesielski, D. E. Stevens, and H. C. Kuo, 1991: Potential vorticity modeling of the ITCZ and the Hadley circulation. *J. Atmos. Sci.*, **48**, 1493–1509.
- Storch, H. V., H. Van Loon, and G. N. Kiladis, 1988: The Southern Oscillation. Part VIII: Model sensitivity to SST anomalies in the tropical and subtropical regions of the South Pacific Convergence Zone. *J. Climate*, **1**, 325–331.
- Tollerud, E. I., and S. K. Esbensen, 1985: A composite life cycle of nonsquall mesoscale convective system over the tropical ocean. Part I: Kinematic fields. *J. Atmos. Sci.*, **42**, 823–837.
- Waliser, D. E., N. E. Graham, and C. Gautier, 1993: Comparison of the highly reflective cloud and outgoing longwave radiation datasets for use in estimating tropical deep convection. *J. Climate*, **6**, 331–353.
- Wallace, J. M., T. P. Mitchell, and C. Deser, 1989: The influence of sea surface temperature on surface wind in the eastern equatorial Pacific: Seasonal and interannual variability. *J. Climate*, **2**, 1492–1499.
- Weare, B. C., 1987: Relationships between monthly precipitation and SST variation in the tropical Pacific region. *Mon. Wea. Rev.*, **115**, 2687–2698.
- Xu, K. M., and K. A. Emanuel, 1989: Is the tropical atmosphere conditionally unstable? *Mon. Wea. Rev.*, **117**, 1471–1479.
- Zhang, C., 1993: Large-scale variability of atmospheric deep convection in relation to sea surface temperature in the tropics. *J. Climate*, **10**, 1898–1913.